JACS
JOURNAL OF THE AMERICAN CHEMICAL SOCIETY
Article
pubs.acs.org/JACS

Extraction of Photogenerated Electrons and Holes from a Covalent Organic Framework Integrated Heterojunction

Mona Calik,[†] Florian Auras,[†] Laura M. Salonen,[†] Kathrin Bader, Irene Grill, Matthias Handloser, Dana D. Medina, Mirjam Dogru, Florian Löbermann, Dirk Trauner, Achim Hartschuh, and Thomas Bein*

Department of Chemistry and Center for NanoScience (CeNS), University of Munich (LMU), Butenandtstrasse 5-13, 81377 Munich, Germany

Supporting Information

ABSTRACT: Covalent organic frameworks (COFs) offer a strategy to position molecular semiconductors within a rigid network in a highly controlled and predictable manner. The π-stacked columns of layered two-dimensional COFs enable electronic interactions between the COF sheets, thereby providing a path for exciton and charge carrier migration. Frameworks comprising two electronically separated subunits can form highly defined interdigitated donor–acceptor heterojunctions, which can drive the photogeneration of free charge carriers. Here we report the first example of a photovoltaic device that utilizes exclusively a crystalline organic framework with an inherent type II heterojunction as the active layer. The newly developed triphenylene–porphyrin COF was grown as an oriented thin film with the donor and acceptor units forming one-dimensional stacks that extend along the substrate normal, thus providing an optimal geometry for charge carrier transport. As a result of the degree of morphological precision that can be achieved with COFs and the enormous diversity of functional molecular building blocks that can be used to construct the frameworks, these materials show great potential as model systems for organic heterojunctions and might ultimately provide an alternative to the current disordered bulk heterojunctions.

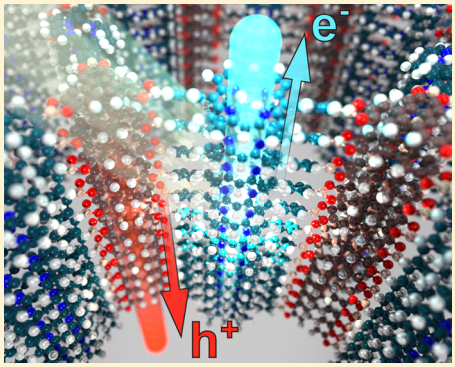

INTRODUCTION

Organic polymer- and small molecule-based solar cells have reached impressive power conversion efficiencies during the past years.[1−4] While much of the progress is stimulated by the development of new donor materials, the precise design of their nanoscale morphology within photoactive blends remains a major challenge.[5−8] Efficient bulk-heterojunction devices require the formation of a bicontinuous network of the donor and acceptor phases with appropriate length scales for charge generation along with favorable molecular packing and long-range order for efficient charge carrier transport.[9−11] It is, however, extremely difficult to predict and control the packing of functionalized conjugated molecules upon spinodal decomposition of a blend solution, as even minor chemical modifications can induce significant changes in the molecular arrangement. Therefore, the generation of an atomically defined interpenetrated three-dimensional (3D) heterojunction via a deterministic bottom-up approach would be a major breakthrough.

Covalent organic frameworks (COFs) are an emerging class of materials featuring molecular building blocks that are organized into 2D or 3D porous crystalline structures through covalent bonds.[12−15] Specifically, the π-stacked aromatic subunits of 2D COFs enable electronic interactions between the COF layers and thus provide a path for exciton and charge carrier transport.[16−20] The rigid COF network provides mechanical and thermal stability, while its optoelectronic properties can be tailored to a specific application via the selection of appropriate building blocks.[21−25] Recently, COFs comprising alternating π-stacked columns of two electroactive building blocks have been reported.[26,27] If the energy levels of these subunits are aligned adequately, an atomically ordered, interdigitated donor–acceptor heterojunction can be formed. Similar to a polymer–fullerene heterojunction, such a material would be expected to promote charge carrier separation upon photoexcitation, thereby presenting an alternative to the present solution-cast disordered photoactive layers. While the photogeneration of charge carriers inside donor–acceptor COFs has been observed in pump–probe experiments,[28] the utilization of this effect in a photovoltaic device has remained elusive to date. Recently, two examples of COF-containing photovoltaic devices have been reported by our group[29] and others.[30] The COFs investigated in those reports, however, did not provide the photoactive junction within their framework but rather served as donor materials when combined with fullerene derivatives as acceptors.

Herein we present for the first time a photovoltaic device that utilizes a vertically oriented thin film of a novel triphenylene–porphyrin (TP-Por) COF as a photoactive donor–acceptor junction. We show that the charge carrier

Received: September 16, 2014
Published: November 20, 2014

   dx.doi.org/10.1021/ja509551m | J. Am. Chem. Soc. 2014, 136, 17802−17807

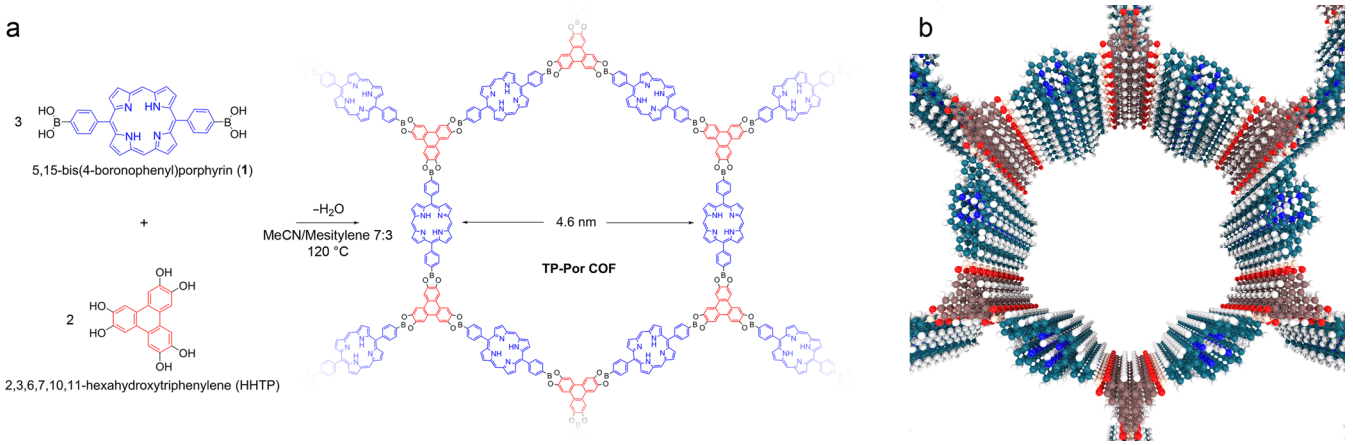

Figure 1. (a) Co-condensation of bis(boronophenyl)porphyrin **1** and HHTP leading to the formation of the layered TP-Por COF. The COF features hexagonal pores with a large diameter of 4.6 nm. (b) Illustration of the TP-Por COF highlighting the alternating columns of triphenylene (red) and porphyrin (blue) subunits.

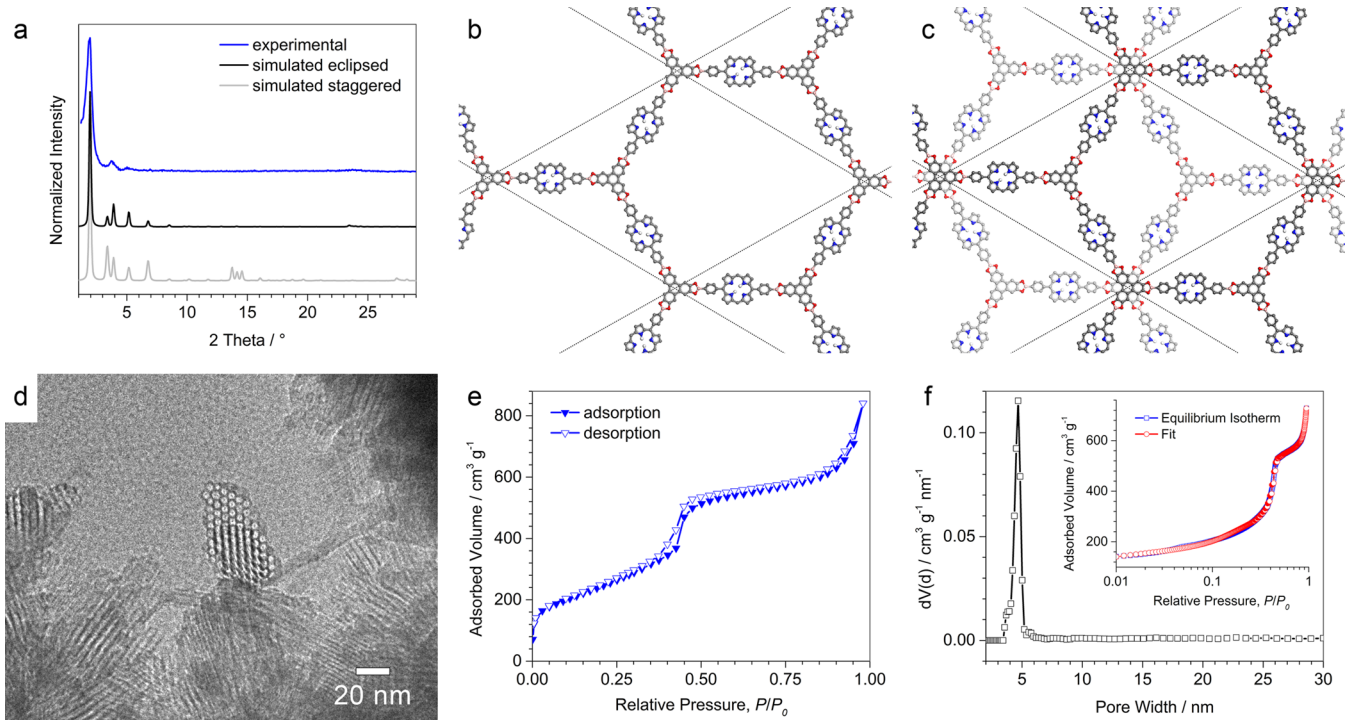

Figure 2. (a) Experimental PXRD data (blue) vs simulated patterns (black and gray) for (b) eclipsed and (c) staggered arrangements of the 2D layers. The theoretical patterns were simulated for a crystallite size of 50 nm. (d) Transmission electron micrograph of TP-Por COF bulk material showing the hexagonal pore structure (middle) and straight porous channels (bottom). (e) Nitrogen sorption isotherm of a TP-Por COF powder sample measured at 77 K. (f) Corresponding pore size distribution with an average pore size of 4.6 nm obtained by fitting the experimental data using a QSDFT equilibrium model (inset).

collection yield can be further enhanced under reverse bias, enabling a peak external quantum efficiency of above 30%.

RESULTS AND DISCUSSION

The new 2D TP-Por COF was formed under solvothermal conditions via co-condensation of 5,15-bis(4-boronophenyl)-porphyrin (**1**) and 2,3,6,7,10,11-hexahydroxytriphenylene (HHTP) in a 7:3 mixture of acetonitrile and mesitylene (Figure 1a; for experimental data, see the Supporting Information (SI)). The TP-Por COF is a porous hexagonal framework with the trigonal triphenylene units at the corners and the linear porphyrins located at the edges (Figure 1b).

Powder X-ray diffraction (PXRD) confirmed the formation of a periodic structure (Figure 2a). The experimental pattern agrees well with the simulated one for an eclipsed (AA stacking) arrangement with *P*3 symmetry (Figure 2b), whereas a hypothetical staggered (AB) layer arrangement cannot reproduce the experimental data (Figure 2c and Figure S1 in the SI). Theoretical calculations carried out for other hexagonal COFs reveal that a slight offset of about 0.1 nm between adjacent layers is energetically favorable.[31] Because of the nonplanar geometry of the porphyrin building block resulting from the large dihedral angle between the porphyrin core and the aryl substituents,[32] a similar or even more pronounced offset for the corresponding COF is anticipated. For the large-

dx.doi.org/10.1021/ja509551m | J. Am. Chem. Soc. 2014, 136, 17802−17807

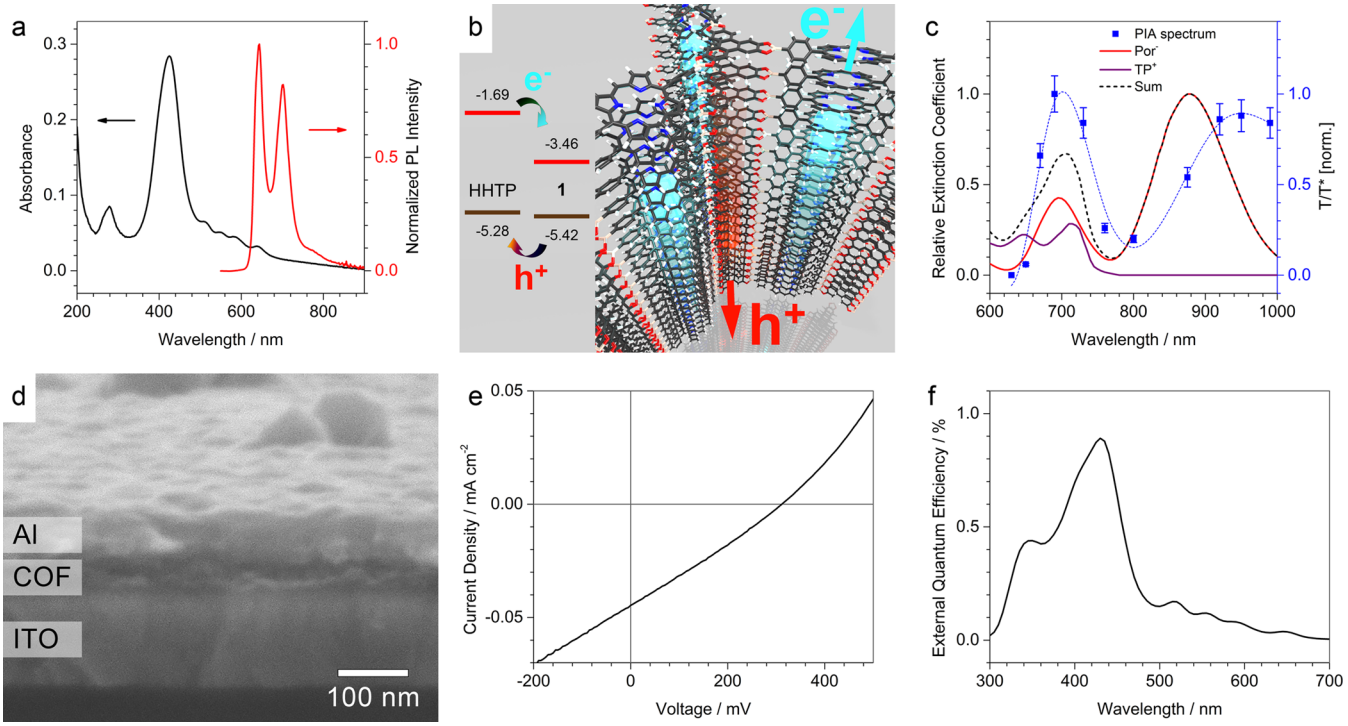

Figure 3. (a) Transmission absorption (black) and normalized PL (λ_{exc} = 405 nm, red) spectra of a TP-Por COF thin film. (b) Frontier orbital energies of the two COF subunits measured by DPV in solution and a schematic illustration of the photoinduced charge transfer. (c) PIA spectrum of the TP-Por COF film after excitation at 470 nm (blue squares; the blue line serves as a guide to the eye) together with the radical ion absorption spectra of Por^{-} (red) and TP^{+} (purple) and their sum (black) assuming a 1:1 ratio of the two species. After photoexcitation, the TP-Por COF film shows two absorption bands in the range of the free radical ion absorption, indicating electron transfer from the donor to the acceptor moiety within the network (see the text). (d) Cross-sectional scanning electron micrograph of a TP-Por COF-based photovoltaic device showing the COF layer between the ITO and Al electrodes. The MoO_x and ZnO contact layers are too thin to be visible in the micrograph. The current–voltage curve (e) and EQE spectrum (f) confirm the successful integration of the donor–acceptor COF as the active layer of the photovoltaic device.

pore TP-Por COF, however, such deviations from a truly eclipsed structure would be sufficiently small (relative to the lattice parameters) to give rise to a nearly identical experimental PXRD pattern. Consequently, experimental PXRD data cannot provide enough evidence for the actual layer offset.

The experimental PXRD pattern of the TP-Por COF exhibits an intense reflection at 2θ = 1.9°, corresponding to a d spacing of 4.6 ± 0.1 nm that can be assigned to the (100) set of crystal planes. The broad reflection at 2θ = 24° corresponds to the (001) planes, indicating an interlayer distance of 0.38 ± 0.02 nm. The larger interlayer distance of the 2D sheets compared with the typically observed packing distance of about 0.35 nm[12] can be rationalized as a result of the nonplanarity of the porphyrin subunit.

Transmission electron microscopy (TEM) images of TP-Por COF powder samples reveal the nanoscale morphology of the framework with crystalline domains of about 50 nm (Figure 2d). Straight porous channels that extend through entire crystal domains are visible for a number of crystallites in the lower part of the TEM image. The hexagonal pore arrangement is evident from domains that are oriented along the crystallographic c axis. We observe a pore-to-pore distance of 5.0 ± 0.3 nm, which is in good agreement with the d spacing obtained from the PXRD measurements.

Nitrogen sorption experiments on TP-Por COF bulk material performed at 77 K yielded isotherms with a typical type IV shape, which is characteristic of mesoporous materials (Figure 2e). The sorption isotherm exhibits a sharp step from P/P_0 = 0.42 to 0.47, indicating a narrow pore size distribution. This was also confirmed by quenched-solid density functional theory (QSDFT) calculations, which showed an average pore diameter of 4.6 nm (Figure 2f). The calculated Brunauer–Emmett–Teller (BET) surface area is 890 $m^2\ g^{-1}$, with a pore volume of 1.1 $cm^3\ g^{-1}$ (for further characterization of the material,[33] see section 6 in the SI).

In order to study the optical properties of the TP-Por COF, thin films were grown on fused silica substrates covered with a 10 nm layer of vacuum-deposited MoO_x. The COF layer was synthesized by immersing the substrates face-down into a dilute reaction solution under otherwise identical reaction conditions (for experimental details see the SI).[34]

The TP-Por COF film exhibits a broad optical absorption covering the entire visible range up to 680 nm with distinct absorption bands that can be ascribed to the triphenylene unit (279 nm) and the porphyrin Soret band (425 nm) and Q bands (510–640 nm) (Figure 3a). Compared with the spectrum of a 2:3 mixture of the reactants, the absorption spectrum of the COF lacks the features of the porphyrin diboronic acid at 300 and 350 nm (Figure S5 in the SI). At longer wavelengths the spectra are nearly identical, indicating similar packing schemes in the COF and in spin-coated films of its building blocks. Upon excitation at 405 nm, both the COF and the porphyrin precursor exhibit a bright red-to-infrared photoluminescence (PL) with two sharp main emission bands at 643 and 701 nm. Depending on the molecular packing arrangement, porphyrins are known to possess different allowed and forbidden optical transitions. Red-shifting of the Soret and Q bands compared with those of highly dilute precursor

dx.doi.org/10.1021/ja509551m | J. Am. Chem. Soc. 2014, 136, 17802–17807

solutions and the existence of sharp PL bands generally indicate the formation of J-aggregates.[35,36] This can be explained by the large aryl substituent−porphyrin core dihedral angle, which hinders the formation of cofacial aggregates. Moreover, the tilted phenyl groups could even facilitate the formation of regular aggregates featuring a small offset between consecutive layers.

Boronate ester-linked COFs typically comprise two electronically different subunits that are arranged into 1D π-stacked columns. If the building blocks are selected in such a way that the HOMO and LUMO energy levels of one component are higher than the respective energy levels of the other component, the COF will form an interdigitated donor−acceptor structure. Similar to polymer−fullerene bulk heterojunctions, an adequately designed COF would be expected to promote charge separation upon photoexcitation of either of its components (Figure 3b). Indeed, the formation of photogenerated charge carriers has been observed on the short time scale of pump−probe experiments in some porphyrin- and phthalocyanine-containing COFs.[28,37] However, the yield of free charge carriers was typically low, and successful extraction of photogenerated charge carriers from a COF layer has not been demonstrated to date.

Electrochemical methods are widely used tools for analyzing the oxidation and reduction potentials of electroactive species. We employed differential pulse voltammetry (DPV) to determine the positions of the highest occupied molecular orbitals (HOMOs) of the precursors relative to ferrocene as an internal standard (Figure S6 in the SI). Assuming $E(\mathrm{Fc/Fc^+})$ = −4.80 eV vs vacuum level[38] and calculating the corresponding lowest unoccupied molecular orbital (LUMO) energies as the sum of the HOMO energy and the optical band gap as determined by UV−vis spectroscopy, we obtain $E_{\mathrm{HOMO}}(\mathrm{TP})$ = −5.28 eV, $E_{\mathrm{LUMO}}(\mathrm{TP})$ = −1.69 eV, $E_{\mathrm{HOMO}}(\mathrm{Por})$ = −5.42 eV, and $E_{\mathrm{LUMO}}(\mathrm{Por})$ = −3.46 eV (Figure 3b). Although these data have been obtained from measurements in solution and the absolute values are expected to shift by a few tens of meV upon crystallization of the COF, we expect the type II alignment of the energy levels relative to each other to remain similar.

On the basis of these results, we expect the TP-Por COF to facilitate photoinduced charge transfer, resulting in the formation of $\mathrm{Por^-}$ and $\mathrm{TP^+}$ radical ions that can be traced via photoinduced absorption spectroscopy (PIA). Indeed, the PIA spectrum of a TP-Por COF thin film exhibits two characteristic absorption bands centered at 700 and 960 nm (Figure 3c). These signals are very similar to the sum of the absorption spectra of the free radical ions of the electron acceptor ($\mathrm{Por^-}$)[39] and donor ($\mathrm{TP^+}$),[40] indicating efficient electron transfer within the framework. Deviations of our experimental spectrum from those in the literature might stem from the different environment of the radical ion species inside the COF.

Growing the COF as a vertically oriented thin film on a suitable electrode and applying an electronically different top contact should enable us to extract photogenerated charge carriers (Figures S2 and S3 in the SI). Thus, we constructed a photovoltaic device with the TP-Por COF as the active layer, sandwiched between indium tin oxide (ITO)/MoO_x and ZnO/Al electrodes. Vacuum-deposited, slightly substoichiometric molybdenum trioxide is commonly used as a hole extraction layer in high-efficiency organic solar cells.[41] Its high work function provides excellent coupling to the HOMO of common donor materials, whereas electron transfer from the LUMO of the acceptor phase is blocked. Zinc oxide has found wide application in organic photovoltaics as an electron-selective contact because of its low work function and good conductivity.[4] For the photovoltaic device, the ∼50 nm thick TP-Por COF layer was grown (as described above) on patterned ITO substrates coated with a 10 nm MoO_x layer. Subsequently, a 20 nm thick ZnO layer was deposited by spin-coating a solution of presynthesized ZnO nanoparticles. The COF film remained unchanged upon the addition of the ZnO layer, as confirmed by UV−vis spectroscopy (Figure S7 in the SI). The devices were completed by thermal evaporation of 70 nm Al electrodes (Figure 3d).

When illuminating the device with simulated solar light, we measured an open-circuit voltage of 312 mV and a short-circuit current density of 44.6 $\mu\mathrm{A\ cm^{-2}}$ (Figure 3e). To the best of our knowledge, this is the first report of a photovoltaic device utilizing the inherent donor−acceptor structure of a COF for photocurrent generation. The importance of the structural precision given by the unique COF geometry is evidenced by a comparison of this device with a reference device based on a randomly intermixed blend of the two building blocks (Figure S9 in the SI). At similar thickness and optical absorption of the active layer, the COF-based device is capable of producing a more than 30 times higher short-circuit current and exhibits an about doubled open-circuit voltage.

In order to further characterize the device, we measured the external quantum efficiency (EQE) under short-circuit conditions (Figure 3f). The EQE spectrum is in excellent agreement with the absorption spectrum of the COF layer, which further confirms the TP-Por COF to be the origin of the observed photoresponse. When the EQE spectrum is plotted on a logarithmic scale, we observe a distinct feature at around 1.55 eV (Figure S8 in the SI). Such sub-bandgap features are commonly observed in organic bulk-heterojunction solar cells and are ascribed to direct photoexcitation of the charge-transfer state. Compared to common polymer−fullerene mixtures, this feature is remarkably sharp, which could be an indication of a more defined charge-transfer state in our morphologically well-defined COF compared with the disordered nature of bulk heterojunctions that are formed through spinodal decomposition.

Although the photocurrent at 0 V bias is promising, the external quantum efficiency is below 1%, indicating the presence of strong loss mechanisms. Sweep-out times of mobile charge carriers as well as the generation of free charge carriers from bound polaron pairs can be greatly enhanced upon application of an electric field having the same direction as the built-in field. Indeed, we observed a dramatically enhanced photocurrent (i.e., the difference between the current under illumination and the dark current) under strong reverse bias. This effect is illustrated by the data in Figure 4a, which we obtained by using chopped simulated solar illumination to continuously switch between the dark and illuminated current density−voltage curves. At V_{appl} = −2 V we observe a difference of about 2 $\mathrm{mA\ cm^{-2}}$ when the light is switched on, which is orders of magnitude higher than the previously reported photoconductivity values for other COFs.[19,37] The EQE under reverse bias can be boosted to more than 30% at 350 nm and well above 10% up to 450 nm (Figure 4b), which renders this COF-based device concept a promising alternative to small molecule/fullerene-containing devices.

dx.doi.org/10.1021/ja509551m | J. Am. Chem. Soc. 2014, 136, 17802−17807

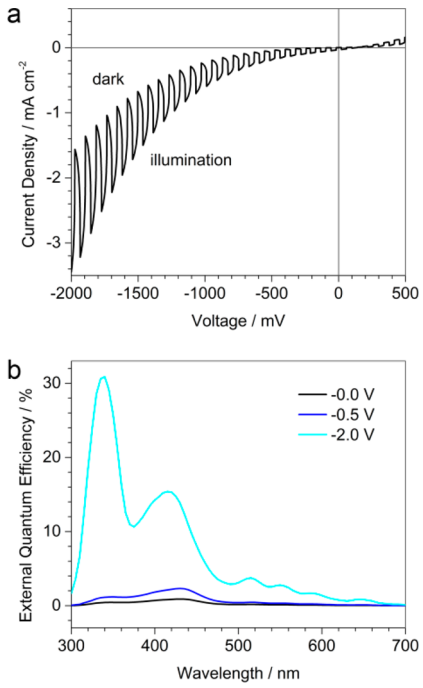

Figure 4. (a) Current density–voltage curves for the photovoltaic device under chopped white-light illumination. (b) Bias-dependent EQE spectra illustrating the greatly enhanced charge collection efficiency under reverse-bias conditions.

CONCLUSION

We have developed a new porphyrin- and triphenylene-containing COF featuring ordered columns of donor and acceptor moieties within its framework. The inherent interdigitated heterojunction of this COF was found to promote charge separation upon photoexcitation of either building block. We applied oriented films of this COF in the construction of the first photovoltaic device in which the COF itself provides the photoactive junction. The structural precision of COF-based heterojunctions presents an opportunity to study charge carrier generation and extraction in well-defined model systems. Quantum efficiency measurements in the presence of an external collection field show the potential of this novel device concept, provided that recombination losses can be minimized. Enhancement of the carrier collection yield that might ultimately lead to competitive device efficiencies is expected from further improvements in the electron and hole transport properties of these materials, a goal we are currently pursuing.

ASSOCIATED CONTENT

Supporting Information

Experimental methods, synthetic procedures, and additional structural and spectroscopic data. This material is available free of charge via the Internet at http://pubs.acs.org.

AUTHOR INFORMATION

Corresponding Author

bein@lmu.de

Author Contributions

[†]M.C., F.A., and L.M.S. contributed equally.

Notes

The authors declare no competing financial interest.

ACKNOWLEDGMENTS

The authors are grateful for funding from the German Science Foundation (DFG; Research Cluster NIM), the Free State of Bavaria (Research Network SolTech), and LMU Munich (LMU Research Fellowship to L.M.S.). The research leading to these results received funding from the European Research Council under the European Union's Seventh Framework Programme (FP7/2007-2013)/ERC Grant Agreement 321339.

REFERENCES

(1) He, Z.; Zhong, C.; Su, S.; Xu, M.; Wu, H.; Cao, Y. *Nat. Photonics* **2012**, *6*, 591.
(2) Hoke, E. T.; Vandewal, K.; Bartelt, J. A.; Mateker, W. R.; Douglas, J. D.; Noriega, R.; Graham, K. R.; Fréchet, J. M. J.; Salleo, A.; McGehee, M. D. *Adv. Energy Mater.* **2013**, *3*, 220.
(3) Chen, S.; Small, C. E.; Amb, C. M.; Subbiah, J.; Lai, T.-H.; Tsang, S.-W.; Manders, J. R.; Reynolds, J. R.; So, F. *Adv. Energy Mater.* **2012**, *2*, 1333.
(4) Kyaw, A. K. K.; Wang, D. H.; Wynands, D.; Zhang, J.; Nguyen, T.-Q.; Bazan, G. C.; Heeger, A. J. *Nano Lett.* **2013**, *13*, 3796.
(5) Liang, Y.; Xu, Z.; Xia, J.; Tsai, S.-T.; Wu, Y.; Li, G.; Ray, C.; Yu, L. *Adv. Mater.* **2010**, *22*, E135.
(6) Guo, X.; Zhou, N.; Luo, S. J.; Smith, J.; Tice, D. B.; Hennek, J. W.; Ortiz, R. P.; Navarrete, J. T. L.; Li, S.; Strzalka, J.; Chen, L. X.; Chang, R. P. H.; Facchetti, A.; Marks, T. J. *Nat. Photonics* **2013**, *7*, 825.
(7) Liu, Y.; Chen, C.-C.; Hong, Z.; Gao, J.; Yang, Y. M.; Zhou, H.; Dou, L.; Li, G.; Yang, Y. *Sci. Rep.* **2013**, *3*, 3356.
(8) Qin, H.; Li, L.; Guo, F.; Su, S.; Peng, J.; Cao, Y.; Peng, X. *Energy Environ. Sci.* **2014**, *7*, 1397.
(9) Peet, J.; Kim, J. Y.; Coates, N. E.; Ma, W. L.; Moses, D.; Heeger, A. J.; Bazan, G. C. *Nat. Mater.* **2007**, *6*, 497.
(10) Ruderer, M. A.; Guo, S.; Meier, R.; Chiang, H.-Y.; Körstgens, V.; Wiedersich, J.; Perlich, J.; Roth, S. V.; Müller-Buschbaum, P. *Adv. Funct. Mater.* **2011**, *21*, 3382.
(11) Westacott, P.; Tumbleston, J. R.; Shoaee, S.; Fearn, S.; Bannock, J. H.; Gilchrist, J. B.; Heutz, S.; deMello, J.; Heeney, M.; Ade, H.; Durrant, J.; McPhail, D. S.; Stingelin, N. *Energy Environ. Sci.* **2013**, *6*, 2756.
(12) Côte, A. P.; Benin, A. I.; Ockwig, N. W.; O'Keeffe, M.; Matzger, A. J.; Yaghi, O. M. *Science* **2005**, *310*, 1166.
(13) Colson, J. W.; Dichtel, W. R. *Nat. Chem.* **2013**, *5*, 453.
(14) Côte, A. P.; El-Kaderi, H. M.; Furukawa, H.; Hunt, J. R.; Yaghi, O. M. *J. Am. Chem. Soc.* **2007**, *129*, 12914.
(15) Kandambeth, S.; Shinde, D. B.; Panda, M. K.; Lukose, B.; Heine, T.; Banerjee, R. *Angew. Chem., Int. Ed.* **2013**, *52*, 13052.
(16) Spitler, E. L.; Dichtel, W. R. *Nat. Chem.* **2010**, *2*, 672.
(17) Wan, S.; Gándara, F.; Asano, A.; Furukawa, H.; Saeki, A.; Dey, S. K.; Liao, L.; Ambrogio, M. W.; Botros, Y. Y.; Duan, X.; Seki, S.; Stoddart, J. F.; Yaghi, O. M. *Chem. Mater.* **2011**, *23*, 4094.
(18) Ding, X.; Feng, X.; Saeki, A.; Seki, S.; Nagai, A.; Jiang, D. *Chem. Commun.* **2012**, *48*, 8952.
(19) Ding, X.; Chen, L.; Honsho, Y.; Feng, X.; Saengsawang, O.; Guo, J.; Saeki, A.; Seki, S.; Irle, S.; Nagase, S.; Parasuk, V.; Jiang, D. *J. Am. Chem. Soc.* **2011**, *133*, 14510.
(20) Patwardhan, S.; Kocherzhenko, A. A.; Grozema, F. C.; Siebbeles, L. D. A. *J. Phys. Chem. C* **2011**, *115*, 11768.
(21) Dogru, M.; Sonnauer, A.; Gavryushin, A.; Knochel, P.; Bein, T. *Chem. Commun.* **2011**, *47*, 1707.
(22) Dogru, M.; Sonnauer, A.; Zimdars, S.; Döblinger, M.; Knochel, P.; Bein, T. *CrystEngComm* **2013**, *15*, 1500.
(23) Wan, S.; Guo, J.; Kim, J.; Ihee, H.; Jiang, D. *Angew. Chem., Int. Ed.* **2008**, *47*, 8826.
(24) Bertrand, G. H. V.; Michaelis, V. K.; Ong, T.-C.; Griffin, R. G.; Dincă, M. *Proc. Natl. Acad. Sci. U.S.A.* **2013**, *110*, 4923.
(25) Spitler, E. L.; Colson, J. W.; Uribe-Romo, F. J.; Woll, A. R.; Giovino, M. R.; Saldivar, A.; Dichtel, W. R. *Angew. Chem., Int. Ed.* **2012**, *51*, 2623.

(26) Feng, X.; Honsho, Y.; Saengsawang, O.; Liu, L.; Wang, L.; Saeki, A.; Irle, S.; Seki, S.; Dong, Y.; Jiang, D. *Adv. Mater.* **2012**, *24*, 3026.
(27) Jin, S.; Furukawa, K.; Addicoat, M.; Chen, L.; Takahashi, S.; Irle, S.; Nakamura, T.; Jiang, D. *Chem. Sci.* **2013**, *4*, 4505.
(28) Jin, S.; Ding, X.; Feng, X.; Supur, M.; Furukawa, K.; Takahashi, S.; Addicoat, M.; El-Khouly, M. E.; Nakamura, T.; Irle, S.; Fukuzumi, S.; Nagai, A.; Jiang, D. *Angew. Chem., Int. Ed.* **2013**, *52*, 2017.
(29) Dogru, M.; Handloser, M.; Auras, F.; Kunz, T.; Medina, D.; Hartschuh, A.; Knochel, P.; Bein, T. *Angew. Chem., Int. Ed.* **2013**, *52*, 2920.
(30) Guo, J.; Xu, Y.; Jin, S.; Chen, L.; Kaji, T.; Honsho, Y.; Addicoat, M. A.; Kim, J.; Saeki, A.; Ihee, H.; Seki, S.; Irle, S.; Hiramoto, M.; Jiang, D. *Nat. Commun.* **2013**, *4*, No. 2736.
(31) Spitler, E. L.; Koo, B. T.; Novotney, J. L.; Colson, J. W.; Uribe-Romo, F. J.; Gutierrez, G. D.; Clancy, P.; Dichtel, W. R. *J. Am. Chem. Soc.* **2011**, *133*, 19416.
(32) Anderson, H. L. *Chem. Commun.* **1999**, 2323.
(33) Smith, M. K.; Northrop, B. H. *Chem. Mater.* **2014**, *26*, 3781.
(34) Medina, D. D.; Werner, V.; Auras, F.; Tautz, R.; Dogru, M.; Schuster, J.; Linke, S.; Döblinger, M.; Feldmann, J.; Knochel, P.; Bein, T. *ACS Nano* **2014**, *8*, 4042.
(35) Peyratout, C.; Daehne, L. *Phys. Chem. Chem. Phys.* **2002**, *4*, 3032.
(36) Li, Y.; Auras, F.; Löbermann, F.; Döblinger, M.; Schuster, J.; Peter, L.; Trauner, D.; Bein, T. *J. Am. Chem. Soc.* **2013**, *135*, 18513.
(37) Feng, X.; Liu, L.; Honsho, Y.; Saeki, A.; Seki, S.; Irle, S.; Dong, Y.; Nagai, A.; Jiang, D. *Angew. Chem., Int. Ed.* **2012**, *51*, 2618.
(38) Frost, J. M.; Faist, M. A.; Nelson, J. *Adv. Mater.* **2010**, *22*, 4881.
(39) Alemán, E. A.; Rocha, J. M.; Wongwitwichote, W.; Mora-Tovar, L. A. G.; Modarelli, D. A. *J. Phys. Chem. A* **2011**, *115*, 6456.
(40) Shida, T.; Hamill, W. H. *J. Chem. Phys.* **1999**, *44*, 4372.
(41) Shrotriya, V.; Li, G.; Yao, Y.; Chu, C.-W.; Yang, Y. *Appl. Phys. Lett.* **2006**, *88*, No. 073508.